Metal-Seeded Growth Mechanism of ZnO Nanowires

Heike Simon, Tobias Krekeler, Gunnar Schaan, Werner Mader[*]

Institute of Inorganic Chemistry, University of Bonn,
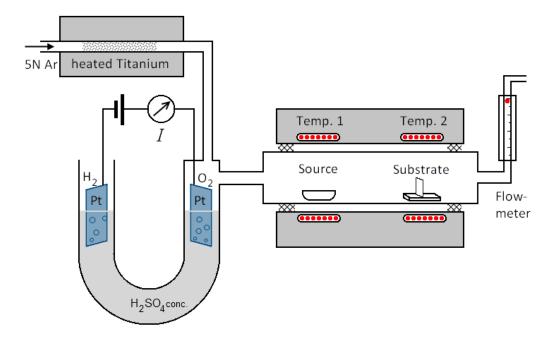Roemerstr. 164, D-53117 Bonn, Germany

Figure S1. Schematic of the thermal CVD growth system. The Ar gas is dried over phosphorous oxide, P_4O_{10}, and CO_2 is removed over KOH (not shown). Finally, the gas is removed from oxygen and nitrogen with a titanium furnace built into the Ar feeding pipe. Oxygen is generated by electrolysis of concentrated H_2SO_4 where the amount of oxygen and hence the partial pressure can be precisely adjusted with the current through the cell. H_2SO_4 as electrolyte prevents degassing of water into the system.
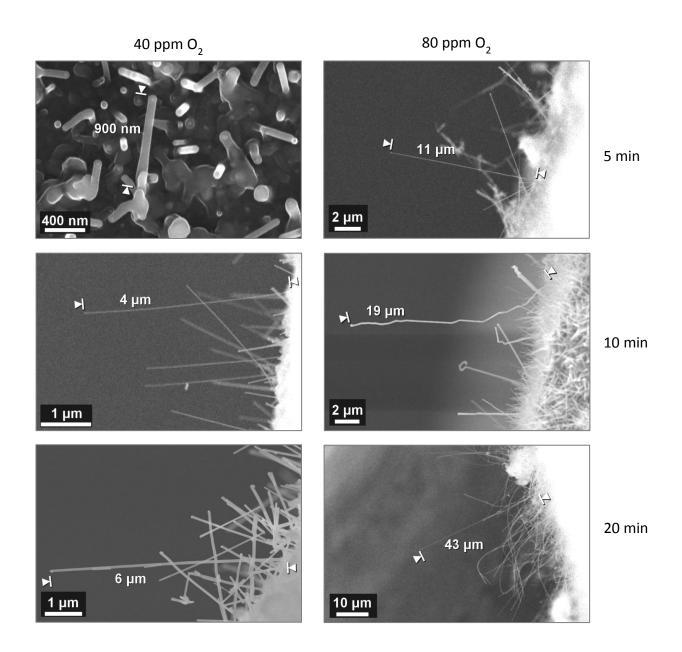
40 ppm O$_2$

80 ppm O$_2$

900 nm

400 nm

11 µm

2 µm

5 min

4 µm

1 µm

19 µm

2 µm

10 min

6 µm

1 µm

43 µm

10 µm

20 min

Figure S2. SEM images of ZnO nanowires grown for different times at 40 ppm O$_2$ (left) and at 80 ppm O$_2$ (right) used for growth rate determination.
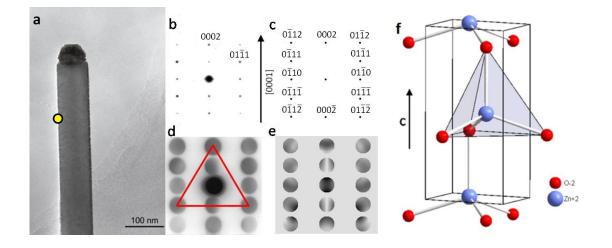
Figure S3. TEM image (a) and corresponding electron diffraction patterns in the *a* axis, <2 $\bar{1}$ $\bar{1}$ 0>, of ZnO. Selected area electron diffraction (SAED) pattern (b) and simulated pattern (c) with indexed diffraction spots. Micro-diffraction pattern (d) taken at the side face of the NW (marked in (a)) and simulated pattern for crystal thickness 75 nm. The intense (0002) reflection and the marked triangle of intense reflections indicate the crystal polarity.[1] Corresponding orientation of the unit cell is shown in (f); the zinc terminated (0001) plane of ZnO faces the Au catalyst.
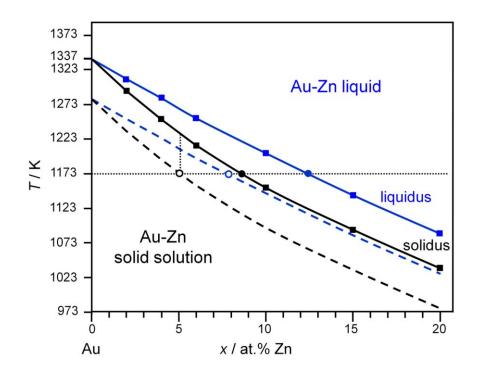

Figure S4. Part of the Au-Zn phase diagram after Okamoto and Massalski [2] (solid lines, square data points) showing limiting liquidus composition of 12.5 at.% Zn at 1173 K. Broken lines schematically illustrate reduction of solidus and liquidus temperatures by 60 K as one possible reason for pre-melting of catalyst surface (open circles).
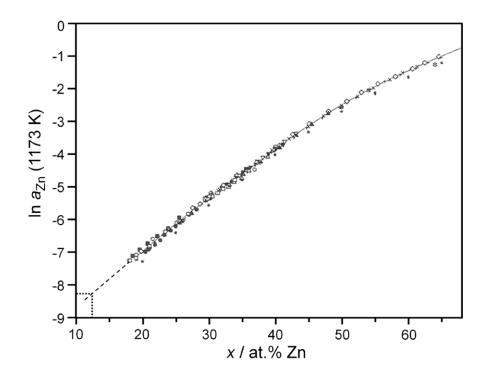
3

Figure S5. Activity of Zn in the liquid Au-Zn phase at 1173 K as function of Zn content with experimental data after Ipser et al.[3] The activity curve is extrapolated for lower Zn concentrations towards the liquidus limit of 12.5 at.% Zn.
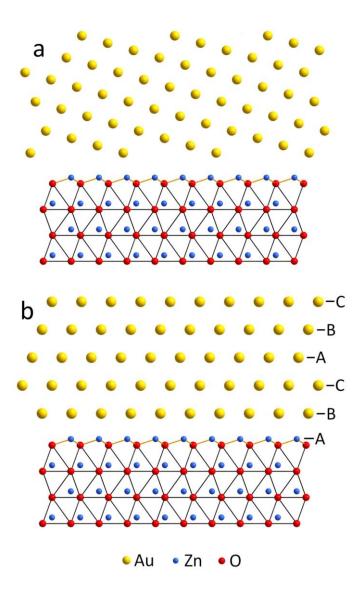
Figure S6. Atomic configurations of Au crystals on a (0001) face of ZnO, unrelaxed models. General interface with a high-indexed plane of gold facing the ZnO NW (a). Special interface with orientation relationship

$$\{111\}_{Au} \parallel (0001)_{ZnO} \quad \text{and} \quad <110>_{Au} \parallel <2\,\bar{1}\,\bar{1}\,0>_{ZnO}$$

where the interface is formed by a {111} plane of Au and the (0001) face of the ZnO crystal, which both are closed-packed planes (b). The general interface in (a) exhibits a low density of contacts with the oxide lattice and hence vacant sites, and good diffusional transport, possibly by vacancy mechanisms, can be imagined. Contrary, the special interface in (b) exhibits a high density of coincidence sites and offers less volume for diffusion of species than the general interface.

Note: the orientation relationship in (b) is the one as observed in Figure 10. Ionic radii are drawn much smaller than space filling radii.
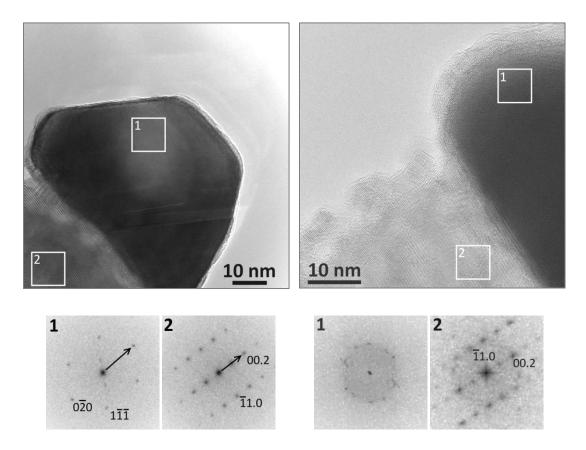
5

Figure S7. Examples of planar interfaces generated by general orientations between Au catalyst and ZnO NW. An inclined four-fold $(200)_{Au}$ plane of the catalyst faces the six-fold $(0001)_{ZnO}$ surface (left). Missing low-indexed reflections in the power spectrum of the Au catalyst typically indicate a general interface between Au catalyst and ZnO NW (right).

References

(1) Mader, W.; Rečnik, A. *phys. stat. sol. (a)* **1998**, *166*, 381–395.
(2) Okamoto, H.; Massalski, T. B. *Bulletin of Alloy Phase Diagrams* **1989**, *10*, 59–69.
(3) Ipser, H.; Krachler, R.; Komarek, K. L. *Zeitschrift für Metallkunde* **1988**, *79*, 725–734.